Novel doping alternatives for transition metal dichalcogenides from high-throughput DFT calculations

Nicolas Onofrio[1]*, David Guzman[2] and Alejandro Strachan[2]

April 3, 2017

[1] Department of Applied Physics, The Hong Kong Polytechnic University, Hong Kong SAR
[2] School of Materials Engineering and Birck Nanotechnology Center Purdue University, West Lafayette, IN 47906 USA

Abstract

Successful doping of single layer transition metal dichalcogenides (TMDs) remains a formidable barrier to their incorporation into a range of technologies. We use density functional theory within the generalized gradient approximation to assess the possibility of substitutional doping the metal and chalcogen sites in molybdenum and tungsten disulfide as well as diselenide against a large fraction of the periodic table. An automated analysis of the energetics, atomic and electronic structure of thousands of calculations results in insightful trends across the periodic table and points out promising dopants to be pursued experimentally. The automated analysis of the electronic structure is able to capture and graphically represent subtleties in the electronic structure of doped TMDs including the presence of gap states and the results are in good agreement with the limited experimental data available. Beyond previously studied cases, our predictions suggest promising candidates for p-type doping and reveal interesting physics behind the doping of the metal site. Doping with early transition metals (TMs) leads to tensile strain and a significant reduction in the bandgap. The bandgap increases and strain is reduced as the d-states are filled into the mid TMs; these trends reverse are we move into the late TMs. Thus, strain and bandgaps are dominated by the non-monotonous variation in atomic radius of the series. Additionally, the Fermi energy increases monotonously as the d-shell is filled from the early to mid TMs and we observe few to no gap states indicating the possibility of both n- (early TMs) and p- (mid TMs) type doping.

Keywords: transition metal dichalcogenides, substitutional doping, density functional theory, high-throughput, carrier concentration

Transition metal dichalcogenides (TMDs) are among the most promising candidates to replace silicon in next-generation, ultrascaled nanomaterials for electronics. As key to their success, two-dimensional TMDs possess a wide range

*Corresponding author: nicolas.onofrio@polyu.edu.hk

of chemical compositions, phases, as well as layer-dependent electronic properties [1]. Breakthroughs in synthesis have enabled a variety of nanodevices [2] including field-effect transistors [3], memories [4], and sensors [5]; even an entire electronic circuit has been proposed based on TMDs and graphene [6]. However, despite the significant promise of TMDs for electronic applications, surpassing silicon-based devices in performance and reliability is challenging and will require progress on several fronts; doping is key among them.

As in bulk semiconductors, controlled doping levels and charge carrier concentrations in single layer TMDs is critical to enable digital electronics. Two major doping strategies have been pursued theoretically and experimentally: *chemical* and *substitutional* doping. Chemical doping consists of the adsorption of atoms or molecules on the surface of the TMD leading to the alteration of its electronic structure as a consequence of surface charge transfer. Javey and coworkers have pioneered this approach and demonstrated p-type conduction in NO_2 doped WSe_2 field effect transistors. The chemisorption of NO_2 acts as surface electron "pumps" and not only affects carrier density but also dramatically lowers the contact resistance with various metals [7]. The second approach, substitutional doping of transition metals (TM) and chalcogen atoms in TMDs has also been recently demonstrated experimentally. For example, p-type conduction has been measured in MoS_2 by substituting Mo with Nb [8] or S with N [9] while strong n-type conduction has been reported when S is substituted by Cl [10]. These doping effects are consistent with simple models based on the change in the total number of electrons in the compound by selecting a dopant having one more or one less electron in its valence shell than the substituted atom. This has been confirmed from first principle calculations showing the Fermi level shifting of chalcogen substituted TMDs with halogen and group V elements [11] as well as TM substitution with Nb [12]. Interestingly, substitutional doping can induce strain to the lattice of TMDs [9], and recent calculations indicate that phase transition can occur upon doping [13]. Despite recent progress, defects and the location of conduction and valance bands results in intrinsic doping of TMDs that is difficult to compensate for [8]. We note that recent research suggests the possibility of healing these defects via oxygen passivation [14]; resulting in substitutional doping.

Substitutional doping has been studied via electronic structure calculations; yet previous studies are limited in the number of substituents studied [12, 15, 16] and there is a need to identify doping trends across the periodic table and across the chemistry of TMDs. We believe such knowledge will contribute to the development of more efficient doping strategies, especially for p-type. In this study, we use density functional theory (DFT) in a high-throughput approach to characterize the energetics, atomic structure and electronic properties resulting from the substitutional doping of the TM and chalcogen sites in Mo and W disulfides and diselenides with every atom in the periodic table. In addition to the known dopants, our calculations show that B, Ge and Sn substitution of the chalcogen atom is promising for p-doping, so is the substitution of Mo by Ti, Zr, Si, Ge, Sn and B elements. N-type doping is more challenging and besides the previously studied dopants we find that V and Nb substitution of the chalcogen atom and Tc doping of Mo show significant promise.

Simulation details. DFT calculations were performed with the SeqQuest package developed at Sandia National Laboratories [17] within the generalized gradient approximation proposed by Perdew, Burke, and Ernzerhof (PBE) [18].

Supercells consist of monolayer TMDs taken in their ground state trigonal prismatic (H-phase) replicated 4×4 times along the in-plane lattice directions, leading to ∼2 % doping concentration when a single atom is substituted. The robust Broyden atomic and cell relaxation algorithm [19] implemented in SeqQuest is key to our methodology, as we found high success rate in the structural relaxations with the simulation achieving the convergence criteria within a relatively small number of steps. Moreover, SeqQuest automatically and exactly eliminates dipole interactions between periodic slab images using the local moment counter charge method [20]. All structures were fully relaxed including lattice parameters and ionic positions until energies, forces and pressure reach values of 0.004 eV, 0.08 eV/Å and 0.2 N/m^2, respectively. A 2×2×1 k-grid was used for integrals in reciprocal space in all simulations. In order to include potential magnetic effects, each doped TMD has been relaxed at various spin states up to 3 (corresponding to spin polarizations 1 to 6). We performed simulations on 4 types of TMDs, including 2 subtitutional sites and 6 spin states and we tested 54 dopants for a total of 2592 simulations. Additionally, we verified that each ground state structure was trigonal prismatic (H-phase) by comparing its energy to the corresponding distorted octahedral structure, often called T' [13]. We also analyzed the final relaxed atomic structures to corroborate whether the substitutional atom remained within the single layer TMD; we found that alkali metals and noble gas do not interact strongly with the host TMD when chalcogen substituted and the final, relaxed position is several Å away from the surface of the monolayer (see Figure S1). Therefore, we will not consider these cases in the following analysis.

We computed the formation energy of each doped TMD as:

$$E_{form} = E_{TOT}^{[MX_2^*+D]} - \left(E_{TOT}^{[MX_2]} - \mu_{sub} + \mu_D\right) \tag{1}$$

with $E_{TOT}^{[MX_2^*+D]}$ the total energy of the doped TMD in its lowest energy spin state, $E_{TOT}^{[MX_2]}$ the total energy of the pristine TMD, μ_{sub} and μ_D the chemical potentials of the substituted atom and the dopant, respectively. These chemical potentials depend on the experimental conditions. We considered two limits for the chemical potential of the substituted atom. In metal-rich conditions, the chemical potential of the metal is set by its ground state crystal structure $\{\mu_M^{M-rich} = \mu_M^0\}$ and the chalcogen is derived assuming equilibrium with the TMD $\{\mu_X^{M-rich} = \frac{1}{2}\left(\mu_{MX_2} - \mu_M^0\right)\}$ with μ_{MX_2} the total energy $E_{TOT}^{[MX_2]}$ per formula unit and μ_M^0 and μ_X^0 the chemical potentials of the metal and chalcogen atoms taken in their standard conditions, respectively. In chalcogen-rich conditions, the chemical potential of the chalcogen is obtained from the di-atomic molecule $\{\mu_X^{X-rich} = \mu_X^0\}$ and that of the metal is derived $\{\mu_M^{X-rich} = \mu_{MX_2} - 2\mu_X^0\}$. The chemical potential of the dopants μ_D were also calculated in their standard conditions.

In order to graphically showcase trends in the electronic structure across the entire periodic table, we developed an algorithm to automatically analyze the electronic density of state (DoS) and extract conduction and valence band edges, Fermi energy and defects within the bandgap. The method starts from a DoS obtained from Kohn-Sham eigenvalues with a gaussian smearing of 0.05 eV. The key steps are summarized as follows:

(i) Starting from the Fermi energy (E_F; evaluated by the DFT code from standard population analysis) we define an energy range [$E_F - \delta$,$E_F + \delta$] that extends well into the valence and conduction bands. The energy parameter should satisfy: $\delta > E_{BG}$ with E_{BG}, the bandgap energy. For our PBE calculations, we choose the value $\delta = 2.0$ eV.

(ii) The DoS is scanned as a function of energy from both ends toward the Fermi energy and the band edges are defined when the density becomes less than a threshold energy E_{thr} (discussed below). For spin-polarized calculations, we consider the averaged spin up and down densities.

(iii) In order to identify defects within the bandgap, the range of energies between the conduction and valence band edges is scanned for densities larger than E_{thr}. For a better detection of defect states in spin-polarized calculations, both spin channels defects are considered.

For validation purpose, we generated all DoS plots and performed a careful comparison with the automated band edge plot. We provide plots of the projected DoS in the Supplementary Material. Our calculations show the best resolution, including the location of band edges and defects with E_{thr}=0.5 eV^{-1}. Moreover, we performed additional simulations with the state-of-the-art HSE06 hybrid functional [21]. We evaluated the uncertainties related to lattice parameter and formation energy to be negligible while we found approximately 20% underestimation of bandgaps, consistent with other study [16]. From the analysis of the electronic structure we noticed that defect states calculated with HSE appear slightly shifted in energy compared to their PBE counterpart resulting in larger energy splitting between defect states in different spin states (see Section S3.1). Finally, we also show Section S3.2 of the Supplementary Material that our PBE formation energies are in good agreement with previous work.

Strain and energetics of doping. Figures 1 and 2 show the formation energy of substituted MoS_2 and $MoSe_2$ calculated in metal- (M-rich: 1a) and chalcogen-rich (X-rich: 1b) conditions as well as the corresponding in-plane strain induced to the lattice, respectively. The figures corresponding to WS_2 and WSe_2 are reported in the Supplementary Material, Figure S2 and S3. M-rich conditions lead to a higher chemical potential for the chalcogen and, consequently, favor substitutional doping of the chalcogen site. Conversely, X-rich conditions favor TM substitutions.

Substitutional doping of Mo (or W) atom with TMs is predicted to be energetically feasible. The formation energies are relatively constant for early TMs and negative in X-rich conditions and increase from mid to late TMs. The associated strain is tensile for early TMs and decreases as we move into the mid TMs; the strain increases again as the d-shell is completed. The induced strain by the TMs and formation energy both follow the non-monotonous trend of atomic radius. In addition to TMs, the predicted energetics show that Mo (and W) could be substituted by other metals and semiconductors except for first row elements (B $\rightarrow$ F). We attribute this effect to their localized 2p electrons being unable to make chemical bonds with the host TMD. Moreover, we found no correlation between Mulliken charges on the substituent and the corresponding formation energies, ruling out significant ionic interactions.

Substitutional doping of the chalcogen atom with other chalcogens as well as group V elements and halogens is predicted to be favorable. For group V, VI,

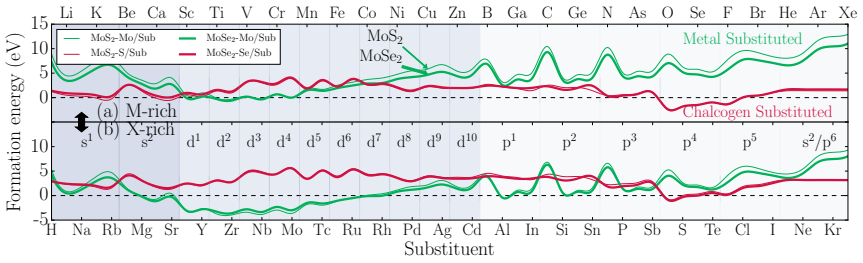

Figure 1: Formation energy of Mo-substituted (green) and chalcogen-substituted (red) MoX_2 (with X=S, Se) in M-rich (a: top) and X-rich (b: bottom) conditions as a function of substituent.

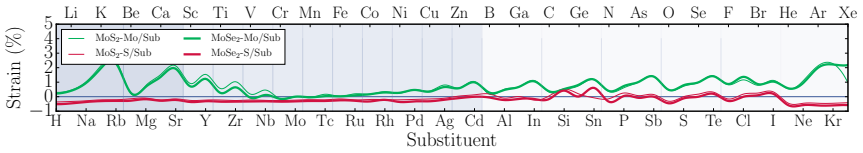

Figure 2: In-plane strain of the lattice consequence of substitutional doping of MoX_2 (X=S, Se) as a function of substituent.

and VII elements, formation energies increase as we move down in the periodic table. This is consistent with the recent demonstration of plasma doping of MoS_2 with N [9]. The formation energies associated with doping the chalcogen site with group III and IV elements are rather constant. The overall strain induced to the lattice by chalcogen doping is slightly compressive, and constant over the entire range of substituents. Finally, we found almost no difference between the energetics and strain of molybdenum and tungsten dichalcogenides.

We note that negative formation energies are not required for doping to be possible since experimental conditions during synthesis can change the chemical potentials of the elements and, consequently, the formation energies. Here we assume that the TMD is isolated and doping occurs between a free-standing sheet and the dopant element taken in its standard conditions. Doping has been reported in various phases; liquid [10], gas [8] and recently plasma [9], conditions that would strongly affect the chemical potential of the dopant. Additionally, it has been demonstrated that the interaction between the TMD and its substrate also plays an important role to doping [22]. Therefore, we will consider in the following potential dopants with formation energies <5 eV.

Electronic structure. Figure 3 shows the conduction band minima (green line) and Fermi energy (red) referenced to the top of the valence band (blue) across the entire set of elements tested. Vertical lines in the bandgap indicate defect states. The figures corresponding to $MoSe_2$, WS_2 and WSe_2 are reported in the Supplementary Material, Figure S4, S5 and S6, respectively. Whether we consider sulfides or selenides, the overall trends including the variation of the bandgap, the Fermi energy and the number of defects are similar. We note however that bandgaps reduce from sulfides to selenides.

We start the discussion with the effect of substitutional doping of the chalco-

gen atom to the electronic structure (top panel of Figure 3a). We found that p-doping can be achieved by incorporation of group V elements in the X-sites, while halogens result in n-type. These results are consistent with prior simulations [12] and we note that our automated analysis captures subtleties in the electronic DoS such as the presence of localized states at the Fermi energy right below the conduction band for halogens (see for example F and I). Moreover, our results are consistent with experimental data of N [9] and Cl [10] doping of MoS_2 resulting in p-doping and n-doping, respectively. In fact, our simulations show that doping $MoSe_2$ or WSe_2 with N should result in improved performance due to a significantly reduced density of gap states. However, we predict a 20% reduction of the bandgap when go down the chalcogen column S→Se. Importantly, doping with B is also predicted to lead to p-type doping for all four cases and one can tune the bandgap by choosing the nature of the TMD. For example, we predict bandgaps of 1.42, 1.38, 1.31 and 1.17 eV for WS_2, MoS_2, WSe_2 and $MoSe_2$ chalcogen substituted with B, respectively. Additionally, some group IV elements also result in p-behavior (Si, Ge, Sn).

Quite interestingly, substitution of the TM leads to significant flexibility both for p- and n-doping. We now focus on the bottom panels of the Figure 3b. The predicted bandgap across the TM family exhibits a maximum for the mid-TMs with reduction into the late and early TMs. This trend can be explained, to a large degree, by the induced strain as tension is known to reduce the bandgap. Thus, the atomic radius of the substituent governs the strain and, as a consequence, the trends in bandgap. The Fermi energy is lowered to the valence band by substitution with early TMs, leading to p-type behavior (Sc, Ti, Zr, V, Nb), which has been already demonstrated experimentally with Nb-doped MoS_2 [8]. As the d-shell is filled, the Fermi energy increases relative to the conduction and valence band edges and we observe a transition from p to n-type doping for mid TMs (Tc, Ru, Rh). Doping with late TMs results in a large number of gap states and, thus, we expect poor transport properties. For example, the substitution of Mo in MoS_2 with Mn creates defects at the Fermi energy, consistent with previous measurements [22].

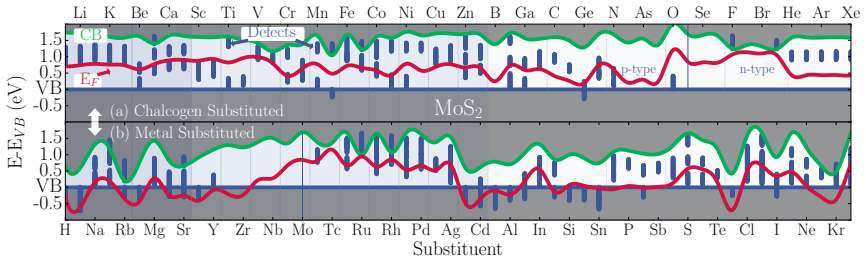

Figure 3: Energy of the conduction band (CB, green), fermi level (EF, red) and defects in the bandgap (BG, blue) with respect to the energy of the valence band (VB, blue line x = 0) of S- (top: a) and Mo- (bottom: b) substituted monolayer MoS_2 as a function of substituents.

Compensating defects can have a strong effect on the ability of engineered defects to change electrical characteristics [23, 24]. In our case, the most likely culprits are TM and chalcogen vacancies and anti-site defects (TM on the chalco-

gen site and vice versa). We will base the discussion on MoS_2 as a representative material, we expect similar behavior in the other cases. The formation energy of Mo vacancies is high (3.7 eV in S-rich conditions and 7.4 eV in Mo-rich conditions) and, thus, is likely unimportant. A sulfur vacancy, V_S, in the neutral state exhibits an empty state about 0.5 eV below the conduction band minima that can trap electrons; thus, limiting n-type doping. Their formation energies (3.2 eV in S-rich conditions and 1.4 eV in Mo-rich conditions) indicate they will be more preponderant that V_{Mo} but healing the vacancy with a halogen would reduce the energy and result in n-type doping. Antisite defects are also relatively high in formation energies. The lowest being S in the Mo site under S-rich conditions with a formation energy of 2.6 eV and could be avoided with less S favorable conditions.

Conclusion. We showed that potential candidates for tuning the carrier density in TMDs are not limited to the substitution with elements that belong to neighboring electronic shell than that of the constituents. Our DFT simulations indicate that group III and IV elements should be explored experimentally to substitute chalcogen atoms and various early TMs are promising to replace Mo/W leading to p-type conduction. Interestingly, we predict that a wide range of bandgaps can be achieved by selecting the nature of boron-doped TMDs. Moreover, we predict improved electronic properties of N-doped transition metal diselenides over sulfides owing to a reduction in gap states. Furthermore, we found that the trends in formation energy and bandgaps of Mo-substituted TMDs correlate with the evolution of atomic radius of TM-dopants. We note that our study focus on the electronic properties of doped-TMDs however, we also predict induced magnetism over a large part of the periodic table elements and we summarize their ground state magnetic moments in Figure S7. Finally, this study can be easily extended to other TMDs, phases and dopants. For example, Er-doped MoS_2 has recently been achieved experimentally giving rise to near-infrared photoluminescence [25].

Supplementary Material

Secs. S1 & S2 show the structural, electronic, and magnetic characterization of Mo- and W-based dichalcogenides. Uncertainties of our calculations are discussed in Sec. S3. The DoS of doped TMDs are provided.

Acknowledgement

This work was partially supported by the FAME and LEAST Centers, two of six centers of STARnet, a Semiconductor Research Corporation program sponsored by MARCO and DARPA. We thank nanoHUB.org and Purdue for the computational resources.

References

[1] Manish Chhowalla, Hyeon Suk Shin, Goki Eda, Lain-Jong Li, Kian Ping Loh, and Hua Zhang. The chemistry of two-dimensional layered transition metal dichalcogenide nanosheets. *Nature Chemistry*, 5(4):263–275, 2013.

[2] Deep Jariwala, Vinod K Sangwan, Lincoln J Lauhon, Tobin J Marks, and Mark C Hersam. Emerging device applications for semiconducting two-dimensional transition metal dichalcogenides. *ACS Nano*, 8(2):1102–1120, 2014.

[3] Branimir Radisavljevic, Aleksandra Radenovic, Jacopo Brivio, i V Giacometti, and A Kis. Single-layer mos2 transistors. *Nature Nanotechnology*, 6(3):147–150, 2011.

[4] Alexander A Bessonov, Marina N Kirikova, Dmitrii I Petukhov, Mark Allen, Tapani Ryhänen, and Marc JA Bailey. Layered memristive and memcapacitive switches for printable electronics. *Nature Materials*, 14(2):199–204, 2015.

[5] Hai Li, Zongyou Yin, Qiyuan He, Hong Li, Xiao Huang, Gang Lu, Derrick Wen Hui Fam, Alfred Iing Yoong Tok, Qing Zhang, and Hua Zhang. Fabrication of single-and multilayer mos2 film-based field-effect transistors for sensing no at room temperature. *Small*, 8(1):63–67, 2012.

[6] Lili Yu, Yi-Hsien Lee, Xi Ling, Elton JG Santos, Yong Cheol Shin, Yuxuan Lin, Madan Dubey, Efthimios Kaxiras, Jing Kong, Han Wang, et al. Graphene/mos2 hybrid technology for large-scale two-dimensional electronics. *Nano Letters*, 14(6):3055–3063, 2014.

[7] Hui Fang, Steven Chuang, Ting Chia Chang, Kuniharu Takei, Toshitake Takahashi, and Ali Javey. High-performance single layered wse2 p-fets with chemically doped contacts. *Nano Letters*, 12(7):3788–3792, 2012.

[8] Joonki Suh, Tae-Eon Park, Der-Yuh Lin, Deyi Fu, Joonsuk Park, Hee Joon Jung, Yabin Chen, Changhyun Ko, Chaun Jang, Yinghui Sun, et al. Doping against the native propensity of mos2: degenerate hole doping by cation substitution. *Nano Letters*, 14(12):6976–6982, 2014.

[9] Angelica Azcatl, Xiaoye Qin, Abhijith Prakash, Chenxi Zhang, Lanxia Cheng, Qingxiao Wang, Ning Lu, Moon J Kim, Jiyoung Kim, Kyeongjae Cho, et al. Covalent nitrogen doping and compressive strain in mos2 by remote n2 plasma exposure. *Nano Letters*, 2016.

[10] Lingming Yang, Kausik Majumdar, Han Liu, Yuchen Du, Heng Wu, Michael Hatzistergos, PY Hung, Robert Tieckelmann, Wilman Tsai, Chris Hobbs, et al. Chloride molecular doping technique on 2d materials: Ws2 and mos2. *Nano Letters*, 14(11):6275–6280, 2014.

[11] Qu Yue, Shengli Chang, Shiqiao Qin, and Jingbo Li. Functionalization of monolayer mos2 by substitutional doping: a first-principles study. *Physics Letters A*, 377(19):1362–1367, 2013.

[12] Kapildeb Dolui, Ivan Rungger, Chaitanya Das Pemmaraju, and Stefano Sanvito. Possible doping strategies for mos2 monolayers: An ab initio study. *Physical Review B*, 88(7):075420, 2013.

[13] Federico Raffone, Can Ataca, Jeffrey C Grossman, and Giancarlo Cicero. Mos2 enhanced t-phase stabilization and sunability through alloying. *The Journal of Physical Chemistry Letters*, 2016.

[14] Junpeng Lu, Alexandra Carvalho, Xinhui Kim Chan, Hongwei Liu, Bo Liu, Eng Soon Tok, Kian Ping Loh, AH Castro Neto, and Chorng Haur Sow. Atomic healing of defects in transition metal dichalcogenides. *Nano Letters*, 15(5):3524–3532, 2015.

[15] Shang-Chun Lu and Jean-Pierre Leburton. Electronic structures of defects and magnetic impurities in mos 2 monolayers. *Nanoscale research letters*, 9(1):676, 2014.

[16] Ai-Ming Hu, Ling-ling Wang, Wen-Zhi Xiao, Gang Xiao, and Qing-Yan Rong. Electronic structures and magnetic properties in nonmetallic element substituted mos 2 monolayer. *Computational Materials Science*, 107:72–78, 2015.

[17] Peter A. Schultz. http://dft.sandia.gov/quest/. also available for online simulations https://nanohub.org/resources/3982.

[18] John P Perdew, Kieron Burke, and Matthias Ernzerhof. Generalized gradient approximation made simple. *Physical Review Letters*, 77(18):3865, 1996.

[19] Charles G Broyden. A class of methods for solving nonlinear simultaneous equations. *Mathematics of Computation*, 19(92):577–593, 1965.

[20] Peter A Schultz. Local electrostatic moments and periodic boundary conditions. *Physical Review B*, 60(3):1551, 1999.

[21] Jochen Heyd, Gustavo E Scuseria, and Matthias Ernzerhof. Hybrid functionals based on a screened coulomb potential. *The Journal of Chemical Physics*, 118(18):8207–8215, 2003.

[22] Kehao Zhang, Simin Feng, Junjie Wang, Angelica Azcatl, Ning Lu, Rafik Addou, Nan Wang, Chanjing Zhou, Jordan Lerach, Vincent Bojan, et al. Manganese doping of monolayer mos2: the substrate is critical. *Nano Letters*, 15(10):6586–6591, 2015.

[23] Ji-Hui Yang, Wan-Jian Yin, Ji-Sang Park, and Su-Huai Wei. Self-regulation of charged defect compensation and formation energy pinning in semiconductors. *Scientific reports*, 5, 2015.

[24] Kirstin Alberi and Michael A Scarpulla. Suppression of compensating native defect formation during semiconductor processing via excess carriers. *Scientific Reports*, 6, 2016.

[25] Gongxun Bai, Shuoguo Yuan, Yuda Zhao, Zhibin Yang, Sin Yuk Choi, Yang Chai, Siu Fung Yu, Shu Ping Lau, and Jianhua Hao. 2d layered materials of rare-earth er-doped mos2 with nir-to-nir down-and up-conversion photoluminescence. *Advanced Materials*, 28(34):7472–7477, 2016.